Slow Chain Dynamics in *Isotactic*-poly(4-methyl-1-pentene) Crystallites near the Glass Transition Temperature Characterized by Solid-State ^{13}C MAS Exchange NMR

Toshikazu Miyoshi,*,† Ovidiu Pascui,‡ and D. Reichert*,‡

Research Center of Macromolecular Technology, National Institute of Advanced Industrial Science and Technology (AIST), Tokyo-Water-Front, 2-41-6 Aomi, Kohto-ku, Tokyo, Japan, and Fachbereich Physik, Martin-Luther-Universität Halle-Wittenberg, 06108 Halle, Germany

Received March 16, 2004; Revised Manuscript Received June 15, 2004

ABSTRACT: The chain dynamics for *isotactic*-poly(4-methyl-1-pentene) (*i*P4M1P) crystallites near the glass transition temperature ($T_g = 304$ K) is characterized by solid-state ^{13}C MAS NMR methods at natural abundance. The ^{13}C line width under high-power proton decoupling and the ^{13}C spin−lattice relaxation time in the rotating frame ($T_{1\rho c}$) detect the segmental motions in the amorphous and crystalline regions with correlation times of about 0.2×10^{-5} s at 360−382 K and about 448 K, respectively. Centerband-only detection of exchange (CODEX) with an additional $T_{1\rho c}$ filter is applied to investigate the motional geometry and kinetic parameters for the main- and side-chain dynamics in *i*P4M1P crystallites in a sample. The CODEX evolution-time dependence of the resolved signals indicates a large-angle reorientational process: the simulation of the experimental data of the main-chain CH_2 signal reveals that *i*P4M1P crystallite performs the helical jump motions with jump angles of 72−145° in the disordered 7_2 helix. The CODEX mixing-time dependence permits the determination of kinetic parameters for the main- and side-chain motions over about 4 orders of magnitude. The determined correlation times for the main-chain carbons match these of the side-chain signals over the investigated temperature range, indicating that the side chain does not perform an independent slow dynamic process in the crystallites. The temperature dependence of the correlation time does not obey an Arrhenius behavior but must be analyzed in terms of WLF behavior with a reference temperature of $T_s = 294$ K. This exceptional behavior of a crystalline material is explained in terms of the amorphous and/or interfacial constraints around T_g. Furthermore, 2-D exchange NMR shows that helical jump motions accompany conformational transition. We also discuss our NMR results in relation to previously reported bulk mechanical relaxation and other data.

Introduction

The mechanical α relaxation in the crystalline region (α_c) for a semicrystalline polymer plays an important role in the bulk material properties such as crystallization, creep, drawability, and probably crystal−crystal transformation. The understanding of the α_c relaxation is, therefore, one of the most important topics in the polymer science field. So far, there are many experimental results and theoretical considerations for the elucidation of the α_c relaxation.[1−12] Among them, advanced two-dimensional (2-D) solid-state exchange NMR methods have been successfully applied to investigate microscopic dynamic nature in the crystallites around the α_c relaxation temperature region.[4−12] Solid-state 2-D exchange NMR observes the molecular dynamics driven reorientation of the ^{13}C chemical shift anisotropy (CSA) or the ^2H quadrupole tensor, which are tightly connected to the atoms and provide detailed information about the geometry of motions and kinetic parameters. For poly(ethylene) (PE),[6] *isotactic*-poly(propylene) (*i*PP),[7,8] poly(oxymethylene) (POM),[8,9] poly(ethylene oxide) (PEO)[5], and *isotactic*-poly(1-butene) (*i*PB),[10,11] the crystalline segments exhibit helical jump motions in the α_c relaxation temperature range. This type of the motion includes a reorientation around the helical chain axis and a translation along its helical axis. In the systems mentioned previously, it was shown that these motions set-in (as detected by NMR) at temperatures well above the glass transition temperature (T_g) and below melting temperature (T_m)[6,9] and that the correlation times or jump rates obey an Arrhenius behavior. It was also shown that the translation motion in the crystalline region leads to chain diffusion between amorphous and crystalline regions,[12−14] meaning that chain dynamics in the crystallites correlates with the dynamics in the amorphous regions. In the present paper, we raise the question as to whether the crystalline dynamics is affected by the constraints of the polymer chain in the amorphous and/or interfacial regions below T_g and if chain dynamics in crystalline segments start near or below T_g.

Kusanagi et al. compiled densities for the amorphous and crystalline regions for polyolefines as a function of the side-chain carbon number.[15] The crystalline density decreases with increasing number of side-chain carbons, while those in the amorphous region are almost independent of the side-chain length. However, *isotactic*-poly(4-methyl-1-pentene) (*i*P4M1P) with a side-chain carbon number 4 shows a unique density character, namely, that the crystalline density is much lower than expected one from an extrapolation of the other materials. It is also lower than that of the amorphous region. We found it therefore interesting to investigate both the molecular structure of *i*P4M1P and the chain dynamics both in the amorphous and in the crystalline regions.

* To whom correspondence should be addressed. (T.M.) E-mail: t-miyoshi@aist.go.jp. Tel: +81-298-61-9392. Fax: +81-3-359-8166. (D.R.) E-mail: reichert@physik.uni-halle.de. Tel: +49-345-55-25593. Fax: +49-345-55-27161.

† Research Center of Macromolecular Technology.

‡ Martin-Luther-Universität Halle-Wttenberg.

10.1021/ma049487c CCC: $27.50
Published on Web 07/29/2004

Structural aspects were investigated by several authors using wide-angle X-ray diffraction (WAXD) and computer simulations. It was found that *i*P4M1P forms disordered 7_2 helical chains, which are packed into a tetragonal unit cell ($a = 18.70$ Å and $c = 13.68$ Å).[15,16] There are abundant experimental results on mechanical properties and dynamics by dynamic mechanical analysis (DMA),[17−22] as well as for PE, *i*PP, and POM. Most of the mechanical data indicated two relaxation processes at 293−323 and 403−433 K. The lower and higher temperature processes were assigned to the α relaxation in the amorphous region (α_a) and α_c relaxation, respectively. Griffith et al. and Reddy et al. reported that the high crystallinity sample shows only lower temperature relaxation[17,21] and proscribed α_c relaxation. The thermal expansion coefficients for crystalline lattices were also utilized to investigate the chain dynamics.[19,23] Nakamae et al. denied any chain dynamics due to an invariance of the thermal expansion coefficient for the *c* axis and elastic modulus.[23] Tanigami et al. showed that the value of the *a* axis slightly changes for the high-temperature region around 423 K and suggested chain dynamics in the crystalline regions.[19]

Several classical NMR techniques were also conducted to investigate the dynamic nature of *i*P4M1P in the wide temperature ranges.[21,24,25] Chan et al. investigated the ^{1}H line width for a highly crystalline sample as a function of temperature and showed that the ^{1}H line width decreases above 318 K.[25] Recently, Reddy et al. concluded from ^{1}H−^{13}C wide line separation (WISE) NMR that the mechanical relaxation at 318 K was not the α_a process but originated from the side-chain motion in the amorphous region.[21] Although many efforts have been performed to understand the dynamic nature for *i*P4M1P in detail, there is no ultimate conclusion about the chain dynamics and no suitable assignment for the mechanical relaxations for *i*P4M1P.

2-D exchange NMR is a convenient tool to investigate the chain dynamics in polymers; however, the necessarily long experimental times prohibit a detailed study of the dynamic processes. Several authors developed 1-D exchange NMR techniques to reduce the experimental time.[26−34] Among them, deAzevedo et al. developed the so-called center-band-only detection of exchange (CODEX) NMR, which is a feasible tool for characterization of polymers with small chemical shift anisotropy (CSA) and different chemically inequivalent carbon nuclei in the monomeric unit.[31,32] In addition, filters based on the different relaxation behavior (spin−lattice relaxation times in the laboratory frame (T_1) and rotating frame ($T_{1\rho}$)) can select crystalline or amorphous signals from the bulk NMR spectrum. Thereby, the combined use of relaxation filters and 1-D exchange NMR enables us to investigate the chain dynamics in the crystalline region unambiguously, even for chemically complicated polymers and in samples of natural isotopic abundance.

In a preliminary paper, we briefly reported CODEX NMR results and concluded that the *i*P4M1P crystallites perform helical jump motions at much lower temperatures than the previously assigned α_c temperature region.[34] In the present paper, we fully analyze the slow-chain dynamics for the *i*P4M1P crystallites. Initially, we show ^{13}C CPMAS NMR spectra and relaxation maps for *i*P4M1P at various temperatures. Second, we shall investigate the motional geometry in the crystalline regions using CODEX NMR. Third, we determine kinetic parameter for chain dynamics in the crystalline regions over 4 orders of magnitude by CODEX. Here, a ^{13}C $T_{1\rho c}$ filter was applied for the suppression of the amorphous signals. We found an exceptional dynamic behavior for crystallite polymer chains near T_g. Finally, we discuss the molecular dynamics obtained from our NMR data in comparison with the previously reported many mechanical and other data.

Experimental Procedures

Sample. *i*P4M1P with an average molecular weight of $M_w = 180\,000$ was purchased from Poly Science Co. Ltd. *i*P4M1P crystallite shows a polymorph of forms I−V, depending on crystallization condition.[35,36] In the present paper, we investigate the chain dynamics for the most stable form I, which can be obtained by isothermal crystallization from the melt,[37] by crystallization from several dilute solutions,[35,36] and by spontaneous crystal−crystal transformation from the unstable form III.[36] In our experiments, we produced a form I-rich sample via crystal−crystal transformation of form III. Initially, a virgin sample was dissolved in a semidilute toluene solvent (0.25 wt %) and was kept for at least 10 h at 378 K. After that, the solution was rapidly cooled in air and evacuated at room temperature. The obtained material was dried for 1 day at room temperature and further dried for another day under vacuum. This resulted in a form III-rich sample that was checked by ^{13}C CPMAS NMR (data are not shown). Form III spontaneously transforms into form I above 333 K. Thus, a form I-rich sample was obtained by heating from the III-rich sample for 1 h at 373 K.

DSC Measurements. DSC measurements were conducted using a Seiko SSC/6000 (DSC 6000) in an N_2 atmosphere with a heating rate of 20 K/min. A crystallinity of 69% was obtained from the ratio $\Delta H/\Delta H_c$, where ΔH is heat of fusion for the sample investigated here, and $\Delta H_c = 61.7$ J/g is that for fully crystalline material.[21,38] Before melting, the DSC curve shows slope change in the range of 290−318 K, which is generally acceptable as the T_g area. The midpoint is 304 K. This assignment will be discussed in the Discussion.

^{13}C CPMAS NMR Measurements. The ^{13}C CPMAS NMR experiments were carried out on a BRUKER AVANCE300 spectrometer, equipped with a 7 mm VT CPMAS NMR probe. The ^{1}H and ^{13}C carrier frequencies are 300.1 and 75.6 MHz, respectively. The MAS frequency was set to 3000 ± 3 Hz. The 90° pulses for ^{1}H and ^{13}C were 4.5−5.0 μs. The recycle delay and cross-polarization (CP) time are 2 s and 1 ms, respectively. High power ^{1}H continuous wave (CW) decoupling was used during the detection period. The chemical shift was referenced to the CH signal of adamantane (29.5 ppm) as an external reference. The temperature in the sample was carefully calibrated by the temperature dependence of the ^{207}Pb chemical shift of $Pb(NO_3)_2$.[39,40] Depending on temperature, 64−256 transients were accumulated. In the dipolar dephasing experiment, an additional delay time with 100 μs after CP was inserted into normal CPMAS experiments. The $T_{1\rho c}$ measurements were performed under a spin-locking field strength of 50 kHz.

^{13}C 2-D MAS Exchange NMR Measurements. 2-D MAS exchange NMR experiments were performed on a BRUKER AVANCE 300 spectrometer, equipped with a 7 mm VT CPMAS NMR probe, and the spectra were obtained by the traditional three-pulse scheme as shown in Figure 1a. The mixing time (t_{mix}) was varied up to 2 s. ^{1}H CW high power decupling and TPPM decoupling[41] were applied for the evolution and detection period, respectively. A total of 320 t_1 increments with a dwell time of 140 μs were acquired. The TPPI procedure was used in the t_1 dimension. The total acquisition time per spectrum was 9−18 h. All the other parameters are the same as for the ^{13}C CPMAS NMR measurements.

CODEX NMR Measurements. The CODEX NMR pulse sequence consists of an exchange and a reference pulse program as shown in Figure 1b,c. The CODEX experiments utilize the recoupling of the CSA interaction by 180° pulses

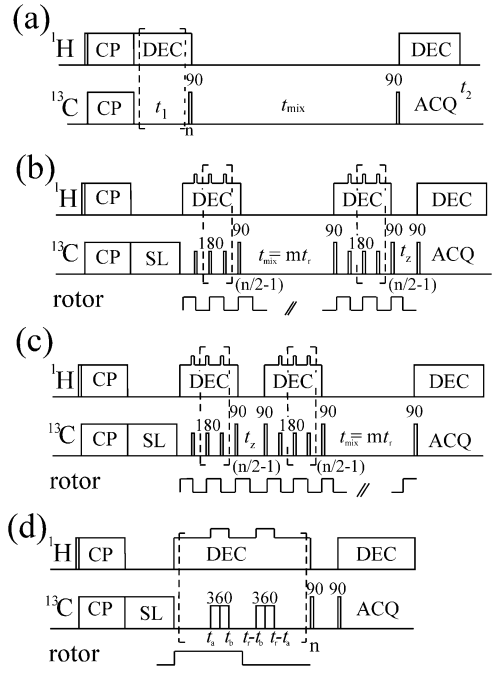

Figure 1. Pulse sequences for ^{13}C 2-D exchange NMR[5] (a), CODEX[31,32] exchange (b), CODEX reference (c), and SUPER[42] (d) used in our investigation. In panels b and c, n =2, 4, 6, ... and panel d, n = 1, 2, 3, ...

trains in the two evolution periods sandwiching a mixing period. The effect is a signal decay due to the dephasing of magnetization brought about by changes in orientation-dependent CSA due to a reorientational dynamic process during t_{mix}.[31−33] The magnetization evolves during the initial evolution period $nt_r/2$ (where n = 2, 4, 6, ...) under the orientation-dependent CSA interaction, which is recoupled by two successive 180° pulses per MAS rotation period, t_r. The magnetization after the first evolution period is stored along the z direction by a 90° pulse and does not dephase during t_{mix} (which must be set to an integer multiple of t_r). The magnetization evolves again after the 90° readout pulse during the second evolution period ($nt_r/2$) and is refocused at its end. The second mixing period t_z serves as a z-filter and permits the cancellation of longitudinal relaxation. In our experiments, t_z was set to one t_r. After applying the last 90° pulse, the signal is detected under ^1H TPPM or CW decoupling. If there is no molecular motion during t_{mix}, the evolutions in the two evolution periods cancel each other out, and there is no decay of the signal intensity. If, however, molecular motion does occur during t_{mix}, the orientation-dependent frequency before and after t_{mix} is different, and thus, the magnetization is not completely refocused. The resulting dephasing leads to a decay of the signal-intensity in the exchange spectrum (S). To remove the T_1 and spin−spin relaxation (T_2) effects during t_{mix} and nt_r, a reference spectrum (Figure 1c) is acquired. It is obtained simply by interchanging t_{mix} and t_z in Figure 1b. The signal intensity in the reference spectrum (S_0) is not sensitive to exchange processes but is only dominated by T_1, T_2, and pulse length errors. The motional correlation time and information about the motional geometry can be obtained by plotting the ratio (S/S_0) versus t_{mix} and (S/S_0) versus nt_r, respectively. A more detailed description of the CODEX experiment can be found in refs 31 and 32. In our experiments, we added a rotor synchronized $T_{1\rho c}$ filter to CODEX pulse program, which suppresses amorphous contributions to S and S_0. The length for the filter was chosen as explained in the main text.

The t_{mix} dependence for CODEX was performed on a BRUKER AVANCE 300 NMR spectrometer, equipped with a 7 mm VT CPMAS NMR. The MAS frequency was 3000 ± 3 Hz. The CP time and recycle delay were 1 ms and 2 s, respectively. The ^1H rf field strength for CW decoupling during ^{13}C 180° pulse with pulse length of 15 μs was set to 80 kHz. The evolution time for CSA was set to 2.2 ms. All other rf parameters were the same as for the CPMAS experiments. The reference and exchange experiments were obtained alternatively by every 128 transients, to suppress drift of the NMR spectrometer. Totally, each spectrum was obtained by accumulating 1024 transients. The total experimental time for mixing-time dependence up to ∼10 s is approx. 40 h.

The Nt_r dependence for CODEX experiment was conducted on Varian Inova 400 with a standard Varian 7 mm VT-CPMAS probe. The ^1H and ^{13}C carrier frequencies were 399.7 and 100.5 MHz, respectively. The MAS frequency is set to 5500 ± 3 Hz. The lengths of the ^{13}C 90° and ^1H 90° pulses are 3.8 and 4.1 μs, respectively. t_{mix} was set to 107 ms. ^1H CW decoupling with a field strength of 65 kHz was used. To suppress the drift of NMR spectrometer, the reference and exchange experiments were obtained by block averaging with a block size of 128 transients. Each spectrum was totally obtained by accumulating 1024 transients. The total experimental time of a typical Nt_r experiment was about 12 h.

CSA Correlation Experiments. To obtain the CSA values of the different chemically inequivalent carbons, an experiment correlating the CSA with the isotropic chemical shifts was employed. In this experiment, the CSA under MAS is recoupled by separation of undistorted quasistatic chemical-shift powder patterns by effortless recoupling (SUPER) (Figure 1d).[42] The SUPER NMR experiment was carried out on a BRUKER AVANCE 300 MHz spectrometer with a 4 mm standard ^{13}C CPMAS NMR probe. The recoupling of CSA under MAS frequency of 3000 ± 3 Hz was achieved by applying four 360° pulses with pulse length of 27 μs in one rotor period, t_r. The timing of two successive 360° pulses is in symmetry with respect to the half rotor period and depends on the rotor period (t_a and t_b were set to 81 and 22 μs, respectively, as shown in Figure 1d). CW and TPPM decoupling were used during t_1 and t_2 periods. The field strength of ^1H decoupling for CW and TPPM and CW during ^{13}C 360° pulses was set to 56 and was 87 kHz, respectively. Before signal detection in the t_2 dimension, a z-filter was used for the suppression of artifacts. In our experiments, we added a rotor synchronized $T_{1\rho c}$ filter to the SUPER pulse program. A total of 64 slice data were acquired along the t_1 dimension with a dwell time of one t_r. Each slice spectrum was accumulated by 128 transients. The phase-sensitive 2-D spectrum was acquired by the States method. The total acquisition time per spectrum was 9 h. All the other parameters were same as for the ^{13}C CPMAS NMR measurements.

Results

^{13}C CPMAS NMR Spectra. Panels a and b of Figure 2 show ^{13}C CPMAS NMR spectra of *i*P4M1P at 299 K, without and with a dephasing time of 100 μs, respectively. The insert shows the disordered 7_2 helical conformations determined by WAXD analysis[15] and the numbering of the carbon atoms. The torsion angles describing C−C bond angles in 7_2 helical conformations were revealed by WAXD analysis (see Table 2 in refs 15 and 43). In the dipolar dephasing technique, the magnetization of ^{13}C spin which directly bonds to ^1H spins, like CH and CH_2, dephase during a relatively short time due to $^1H-^{13}C$ heteronuclear dipole interaction. On the other hand, CH_3 and quaternary carbons that have weak $^1H-^{13}C$ dipolar interactions require a much longer time for magnetization dephasing. Therefore, we can selectively observe two methyl signals of C5 and C6 in *i*P4M1P in the dipolar filter experiment. The dipolar dephasing NMR spectrum shows two separated signals. The observed isotropic chemical shift (σ_{iso}) difference between C5 and C6 signals should be attributed to the conformational effects. The C6 carbons have torsion angles of 81−99° with respect to the main chain CH carbon (C2) in the γ position, whereas C5 has the angles of −141 to −172° with respect to the C2 one

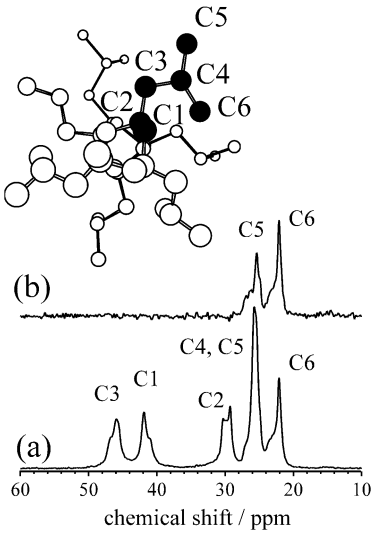

Figure 2. (a) ^{13}C CPMAS NMR spectra of *i*P4M1P without (a) and with (b) dipolar dephasing of 100 μs. The 7_2 helical structures for *i*P4M1P crystallite (view down the *c* axis) determined by WAXD method,[15] and NMR signal assignment is shown as an insert.

Table 1. ^{13}C Isotropic Chemical Shift (σ_{iso}) Values and Principle Values for CSA of *i*P4M1P Crystallites Measured at 299 K[a]

	σ_{iso}	σ_{11}	σ_{22}	σ_{33}
C1	41.8	63	40	22
C2-1	29.3	41	28	21
C2-2	30.3	41	28	22
C3	46.0	66	49	24
C4[b]	25.7	32	26	20
C6	22.1	33	27	7

[a] Principle values for CSA of *i*P4M1P crystallites were obtained by SUPER method. The experimental errors are within ±3 ppm. [b] We cannot measure CSA pattern of C5 signal due to overlapping of C4 one.

in the γ position. The former is relatively close to the gauche position, while the latter is approximately a trans conformation. Therefore, the observed upfield shift for the C6 carbon should be attributed to a γ gauche effect.[44,45] The observed difference between C5 and C6 signals shows that the side-chain motion around the C3−C4 bond is restricted and slower than the σ_{iso} difference of 272 Hz.

The other signal assignments are also inserted into Figure 2, and the obtained σ_{iso} values are listed in Table 1. The signals also show asymmetric line shapes for the main chain CH_2 (C1), side-chain CH_2 (C3), C5, and C6 and doublet line shape with a separation of 1.0 ppm for the C2 signal. There are two possible reasons for such asymmetric and doublet line shapes: conformational and packing effects. Previously, Reddy et al. attributed the observed asymmetric and doublet line shape for C2 to packing effects.[21] Separately, Rosa et al. investigated both effects of conformation and packing on NMR chemical shifts for each carbon for form I−IV of *i*P4M1P.[43] The latter revealed that the chemical shift of the C2 carbon in a series of forms I−IV depends on the torsion angles of the main chain, and the asymmetric line shapes for C5 and C6 signals were attributed to the different distances (packing effect) from the side-chain carbons in the neighboring chains. However, in the case of form I, C5 and C6 carbons also show distribution of torsion angles with respect to the C2 carbon in the γ positions. Therefore, conformational effects should also contribute to the observed line shape for C5 and C6 signals.

Figure 3 shows ^{13}C CPMAS NMR spectra of *i*P4M1P as a function of temperature. With increasing temperature, the C2 doublet signals merge into a singlet around 382 K. Similarly, the other signals also show line-shape change in the same temperature region. Furthermore, the σ_{iso} values of all signals move downfield with increasing temperature. The observed changes are reversible with temperature and imply that conformational and packing structural changes occur with increasing temperature. The signals show apparent line broadening above 404 K. Moreover, the narrowed signals for the C1, C2, C3, and C6 carbons as marked by asterisks appear on top of the broad crystalline signals. We performed line-shape analysis by fitting Lorentzian functions to the experimental data above 428 K. Two components are applied for line fitting to the C1, C2, C3, and C6 signals. The fitted curves for the C1, C2, and C3 signals are shown in Figure 3. Within the investigated range, the broadened components have their maximum line widths at 448 K. Under ^{1}H dipolar decoupling (DD) condition, the ^{13}C line width becomes largest if the correlation time of a motion reaches inverse of ^{1}H DD field strength (0.2×10^{-5} s).[46,47] Further shortening of the correlation time induces a renarrowing of the line width. Therefore, the broadened C1, C2, and C3 signals show that correlation times for the segmental motions in the crystalline region are close to 0.2×10^{-5} s at 448 K. The narrowed signals (dotted curves) must be attributed to the amorphous ones, meaning that the amorphous segments are much more mobile than those for the crystalline segments and have much shorter correlation times than 0.2×10^{-5} s. More details will be discussed in the next section.

^{13}C Spin-Lattice Relaxation Time in the Rotating Frame, $T_{1\rho c}$. The spin-lattice relaxation time in the rotating frame ($T_{1\rho c}$) is sensitive to motions in the mid 10 kHz range; therefore, it has been utilized for the detection of the segmental motions above T_g.[48,49] Actually, the observed $T_{1\rho c}$ decay curves contain information about the motional process including frequency, amplitude, and anisotropy of motions as well as undesired contributions from fluctuations of dipolar field due to mutual ^{1}H−^{1}H flip−flop processes[48−50] that may complicate the interpretation of $T_{1\rho c}$ in rigid samples. However, the signals in the amorphous and crystalline regions evidently show ^{13}C motional narrowing and broadening, respectively. Therefore, we safely assume that the significant contribution to the observed $T_{1\rho c}$ is dominated by the motional process except for very low temperatures. We measured $T_{1\rho c}$ for all the resolved carbons in *i*P4M1P at various temperatures. The obtained relaxation curves are analyzed in terms of single and double exponential functions. The relaxation values and the share of the short $T_{1\rho c}$ for all signals are listed in Table 2. We carefully adjusted the experimental conditions according to the relaxation values for the main-chain signals to observe the main-chain dynamics in the crystalline and amorphous regions.

The experimental data and best fit curves for the C1 signal are shown in Figure 4 a. At 299 K, the $T_{1\rho c}$ values of the short and long components are 3.0 ± 0.6 and 31.2 ± 2.4 ms, respectively. We display two ^{13}C CPMAS NMR spectra with different spin-locking times of 0.01 and 10 ms in Figure 4b. The latter spectrum is multiplied by a scaling factor of 1.28, which was estimated from a

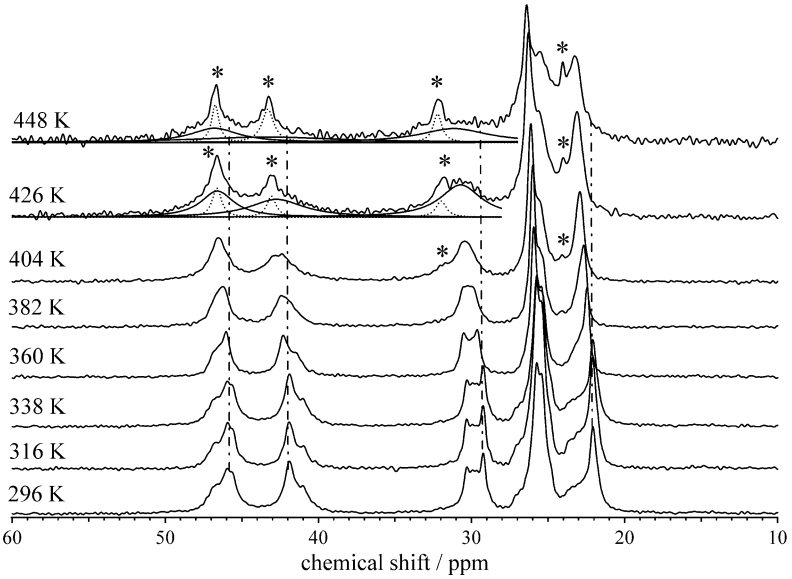

Figure 3. ^{13}C CPMAS NMR spectra of *i*P4M1P at various temperatures. The asterisk marks show the amorphous signals.

Table 2. ^{13}C Spin Lattice Relaxation Time in the Rotating Frame ($T_{1\rho c}$) for the Resolved Signals for *i*P4M1P at Various Temperatures[a]

	C1	C2	C3	C4, 5	C6
258 K	2.0 ± 1.2 (0.12)	3.0 ± 0.9 (0.14)	5.3 ± 0.6 (0.20)	>100[b]	>100[b]
	48.2 ± 1.4	99.2 ± 10.3	60.3 ± 4.4		
288 K	2.6 ± 1.2 (0.17)	5.1 ± 1.4 (0.18)	10.1 ± 2.0 (0.25)	>100[b]	>100[b]
	45.3 ± 2.4	80.4 ± 7.3	97.2 ± 10.3		
299 K	3.0 ± 0.6 (0.18)	2.1 ± 0.3 (0.16)	4.5 ± 1.1	>100[b]	>100[b]
	31.2 ± 2.4	51.4 ± 2.3	49.4 ± 4.6		
316 K	3.7 ± 0.6 (0.16)	2.0 ± 0.4 (0.20)	2.2 ± 0.4	75.4 ± 9.8	>100[b]
	31.4 ± 3.7	46.6 ± 5.2	49.3 ± 4.5		
338 K	2.0 ± 0.2 (0.12)	1.5 ± 0.2 (0.13)	35.3 ± 4.3	66.2 ± 8.3	>100[b]
	26.4 ± 2.6	21.8 ± 1.3			
360 K	13.3 ± 0.6	21.6 ± 1.2	28.4 ± 1.4	59.4 ± 4.4	>100[b]
382 K	6.7 ± 0.3	12.2 ± 1.2	12.3 ± 1.3	37.3 ± 3.5	72.3 ± 10.4
448 K	0.5 ± 0.1 (0.27)	1.0 ± 0.2 (0.38)	1.4 ± 0.2 (0.45)	2.5 ± 0.2 (0.42)	5.1 ± 1.2 (0.45)
	9.2 ± 1.1	15.2 ± 1.1	15.9 ± 1.7	13.7 ± 0.7	23.9 ± 6.6

[a] The component ratio for short $T_{1\rho c}$ is shown in parentheses. [b] The $T_{1\rho c}$ value is much larger than 100 ms. Our spin-locking time is 45 ms, which is not sufficient to determine $T_{1\rho c}$ values longer than 100 ms.

relaxation factor of 1/(exp −10/41 ms). The value of 41 ms is an average of the large values of C1 and C2 at 299 K. The difference spectrum between the two spectra is also shown in Figure 4b, showing much broader signals for the C1, C2, and C3 signals as compared to the bulk ones. These broad signals should be assigned to the ones for the amorphous region. At 360−382 K, only one $T_{1\rho c}$ component showing the crystalline signal is observed for the C1 signal (Figure 4a). The amorphous signal disappears due to shortening of the $T_{1\rho c}$ value. With a further increase in temperature, the crystalline signals become broader, and the narrowed amorphous signals appear on the crystalline signals above 404 K (Figure 3). At 448 K, the spectra with different spin-locking times (0.01 (solid curve) and 4 ms (broken curve)) and difference spectra are shown in Figure 4c. The narrowed C1 signal in the amorphous region shows a long $T_{1\rho c}$ value of 9.2 ± 1.1 ms, whereas the broadened signal for the crystalline region has a short value of 0.5 ± 0.1 ms, which is close to a minimum value for $T_{1\rho c}$.[51] It should be noted that the C2 and C3 signals also show a similar temperature dependence of $T_{1\rho c}$ values with the C1 ones. From these results, we can roughly estimate that the segmental motions in the amorphous and crystalline regions have motional frequencies of mid-10 kHz at around 360−382 and near 448 K, respectively.

On the basis of the obtained $T_{1\rho c}$ results, we use a ^{13}C $T_{1\rho c}$ filter for the selective observation of the crystalline signals in the CODEX and SUPER experiments. The ^{13}C $T_{1\rho c}$ filter lengths at 258, 299, 305, 315, 327, and 338 K are 15, 7, 7, 5, 5, and 3 ms, respectively. Above 338 K, we do not use a relaxation filter in the CODEX experiments.

2-D MAS Exchange NMR. The 2-D MAS exchange NMR is sensitive to exchange between the different σ_{iso} values. We measured 2-D MAS exchange NMR spectra of *i*P4M1P crystallites with a different t_{mix} at 360 K. The ^{13}C 2-D exchange CPMAS NMR spectra of the C2 signal with t_{mix} of 2 and 500 ms are shown in Figure 5a,b, respectively. For t_{mix} = 2 ms, only diagonal signals are observed, while with increasing t_{mix}, characteristic exchange peaks appear, and the intensity almost reaches an equilibrium state at t_{mix} = 500 ms (Figure 5b). The other signals also show strong off diagonal intensities under t_{mix} = 500 ms (data are not shown), indicating that the asymmetric line shapes for C1, C3, C4, C5, and C6 originate from the same reason as for the C2 signal. This 2-D result proves that conformational transition occurs in the crystalline region at 360 K. We plotted the exchange intensity ($I_{off\ diagonal}/I_{diagonal}$) for the C2 carbon as a function of t_{mix} in Figure 5c. The exchange intensity increases up to a plateau of 0.65, and the exchange curve shows nonsingle exponential behavior and was

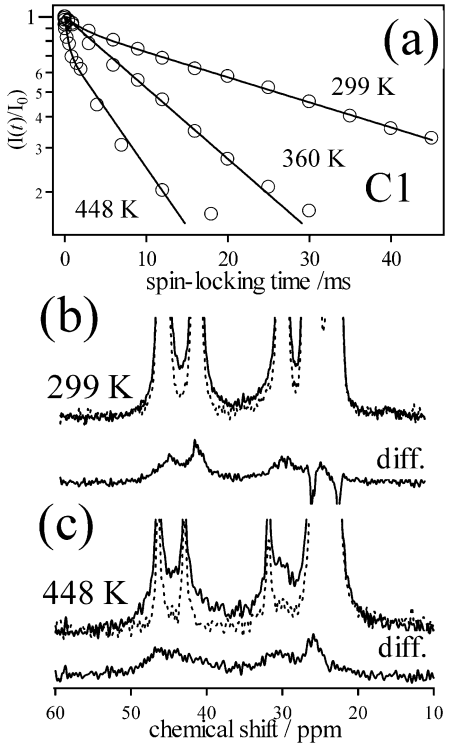

Figure 4. Relaxation decays for ^{13}C spin−lattice relaxation time in the rotating frame ($T_{1\rho c}$) for C1 (○) signal measured at 299, 360, and 448 K. The solid curves show the best fitted one to the experimental data using single or double exponential functions. (b) The ^{13}C CPMAS NMR spectra with spin-locking times of 0.01 (solid line) and 10 ms (broken line) and difference spectrum (solid line) at 299 K. The former two spectra were cut at the intensity of 25% of the highest signal intensity. (c) The ^{13}C CPMAS NMR spectra with spin-locking times of 0.01 (solid line) and 4 ms (broken line) and difference spectrum (solid line) at 448 K. The former two spectra were cut at the intensity of 35% of the highest signal intensity.

fitted to the equation

$$(I_{\text{off diagonal}}/I_{\text{diagonal}}) = p(1 - \exp(-(t_{\text{mix}}/\tau_c)^{\beta})) \quad (1)$$

where p, τ_c, and β are the population of the mobile groups, the correlation time, and the KWW distribution width, respectively. The solid curve is the best fit to the experimental data with fitting parameters of $p = 0.64 \pm 0.01$, $\tau_c = 59.5 \pm 5.1$ ms, and $\beta = 0.63 \pm 0.04$. The β value corresponds to a distribution width is 0.7 decade.[52] We like to mention that we performed a spin-diffusion correction prior to the fitting. The spin-diffusion correction curve is the same to that in the CODEX experiments. Details will be discussed later.

Geometry of Motion. We apply the CODEX experiment for a further characterization of the dynamic process that leads to ^{13}C line broadening and conformational transition in the crystalline region. Figure 6 shows CODEX exchange and reference NMR spectra, respectively, with an evolution period of 2.2 ms and $t_{\text{mix}} = 107$ ms at 360 K. t_{mix} is longer than the correlation time for the conformational transition. The signal intensities for the side-chain signals C3 and C6 as well as the main-chain signals C1 and C2 in the exchange spectrum (S) are much smaller as compared to those in the reference spectrum (S_0). The Nt_r dependence of (S/S_0) for all the resolved signals at $t_{\text{mix}} = 107$ ms and 333 K is shown in Figure 7 a. The error bars are obtained from the signal-to-noise ratios of the exchange and reference spectra. For all the signals, the error-bar sizes increase with increasing Nt_r, mainly due to effects of the spin−spin relaxation time, T_2, and increased intensity losses due to increasing number of p pulses. The (S/S_0) intensities of the signals except for overlapped signals of C4 and C5 reach plateaus within Nt_r of 2.2 ms. The slow decay of the overlapped C4 and C5 signals are due to the small CSA principal values of C4 carbon. The CSA principal values (σ_{11}, σ_{22}, σ_{33}) of the carbons were obtained by the SUPER method.[42] Sheared 1-D slices for all the resolved signals multiplied with a spectral scaling factor of 0.155 are shown in Figure 8; the extracted principal values are also listed in Table 1. Therefore, these CODEX data in Figures 6 and 7a tell us that overall chain dynamics in the crystalline region occurs on a time scale shorter than 107 ms at 333 K. Since the polymer chains in the crystalline lattice are packed into the lattice, the motional degrees of freedom are highly restricted in the crystallites. The most plausible and obvious chain dynamics is a rotation around their chain axes.

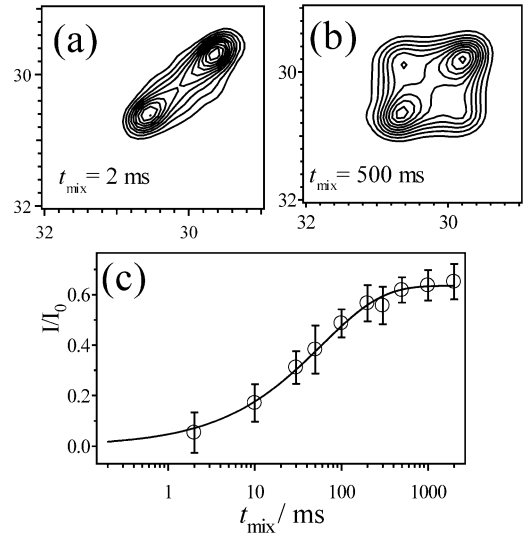

Figure 5. Expanded regions of ^{13}C 2-D exchange NMR spectra for the C2 signal of *i*P4M1P crystallites with t_{mix} of 2 ms (a) and 500 ms (b) measured at 360 K. (c) t_{mix} dependence of the off diagonal/diagonal intensity ($I_{\text{off diagonal}}/I_{\text{diagonal}}$) ratio for C2 carbon (○) of *i*P4M1P crystallite. The error bars are signal-to-noise ratios of the diagonal and off diagonal peaks. The solid curve was the best fitted one to the experimental data using $p(1 - \exp(-(t_{\text{mix}}/\tau_c)^{\beta}))$, where p, β, and τ_c are a fraction ratio that participate in exchange, KWW distribution parameter, and correlation time, respectively. The obtained best fitted parameters with $p = 0.64 \pm 0.01$, $\tau_c = 59.5 \pm 5.1$ ms, and $\beta = 0.63 \pm 0.04$.

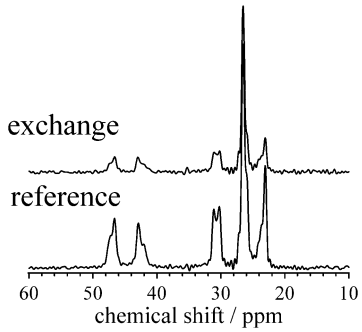

Figure 6. ^{13}C CODEX exchange and reference NMR spectra of *i*P4M1P crystallites, with $t_{\text{mix}} = 107$ ms and recoupling time of 2.2 ms under MAS frequency of 3000 ± 3 Hz, measured at 360 K.

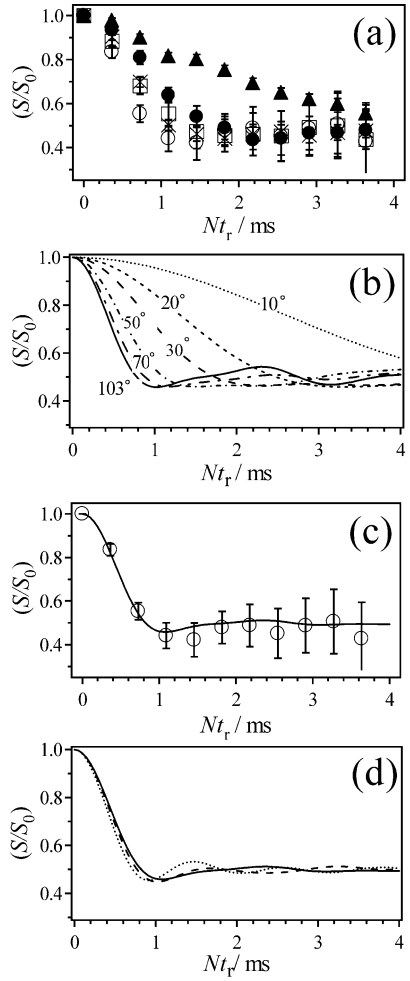

Figure 7. (a) ^{13}C CODEX experimental results of (S/S_0) intensities for C1 (○), C2 (●), C3 (□), C4, C5 (▲), and C6 (×) for *i*P4M1P crystallite with t_{mix} = 107 ms under a MAS frequency of 5500 ± 3 Hz, obtained at 333 K. (b) Simulated curves for jump motion with jump angles of 10° (dotted), 20° (short-dashed), 30° (long-dashed), 50° (short-dashed and dotted), 70° (long-dashed and dotted), and 103° (solid) around their helical axes in an uniform 7_2 helix. (c) The solid curve is the average of the simulated curves for jump angles with 122, 84, 93, 145, 96, 72, and 109° in the disordered 7_2 helix and the evolution time dependence of (S/S_0) for C1 signal (○). (d) The dotted and broken curves show the simulated ones for averaged 7_2 helical jump motions assuming σ_{22} deviation from common direction by +30 and −30°, respectively. For comparison, the simulated averaged jump without deviation of tensor direction is also plotted as a solid curve.

To verify this assumption, we numerically simulate the CODEX curve of C1 signal due to molecular motions. We require information about CSA principal axis direction (X^{PAS}, Y^{PAS}, Z^{PAS}) and Euler angles, which describe reorientation of CSA tensor due to molecular motions. In synthetic polymers, the main-chain CH_2 carbon shows common CSA principal direction due to C−CH_2−C symmetry as the following:[53,54] σ_{33} is orthogonal to the CH_2 plane (Z^{PAS}), σ_{22} is along the bisecting direction of the CH_2 angle (Y^{PAS}), and σ_{11} is orthogonal to both the σ_{22} and σ_{33} directions (X^{PAS}). We assume that the C1 carbon of *i*P4M1P shows this common direction. The orientations of PAS before and after rotations are convincingly described in terms of rotation of PAS in MF (X^{MF}, Y^{MF}, Z^{MF}), where the helical axis is Z^{MF} axis. In the case of the uniform helix, the orientations of PAS before and after rotation is due to Euler angles, (α, β, 0) and (α, β, ψ), respectively, where β is angle between Z^{PAS} and Z^{MF}, and α is the angle of the rotation of the Y^{PAS} axis around the Z^{PAS} axis onto the node line, which is perpendicular to Z^{PAS} and Z^{MF}, and ψ is the rotational angle.

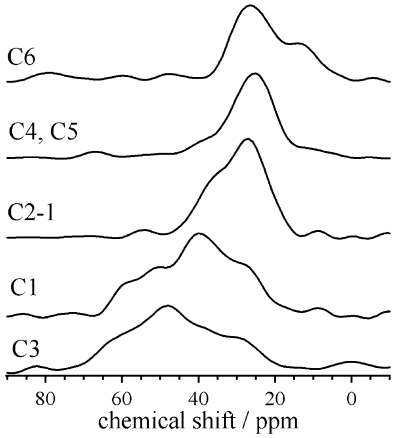

Figure 8. ^{13}C CSA slice spectra from a 2-D SUPER spectrum of *i*P4M1P crystallites taken under MAS frequency of 3000 ± 3 Hz at 299 K. The chemical shift of the slice spectra were scaled by a factor of 0.155. For C2 carbon, one of the doublet signals at 29.3 ppm (C2-1) is shown.

Initially, if we consider the effect of the jump angle on the CODEX attenuation curves in uniform 7_2 helix, the Euler angles (α, β) of C1 carbon are calculated using a trigonal relation to be (81°, 40°) from the atomic positions determined by WAXD[15] and the PAS direction fixed to the atom in MF.[5] The simulated CODEX attenuation curves with jump angles of 10, 20, 30, 50, 70, and 103° are shown in Figure 7b. The helical jump angle between the neighboring sites is 360° × 2/7 = 103°. It is evidently shown that CODEX attenuation strongly depends on the jump angle and that large amplitude motion of 70−103° induces the steep decay for (S/S_0) in the initial period.

Actually, *i*P4M1P crystallites show slightly disordered 7_2 helical conformations in the lattice. Therefore, jump angles between the seven neighboring sites deviate from 103° and are 122, 84, 93, 145, 96, 72, and 109°.[15] We calculated the CODEX dephasing curve for each jump angle. The average one and the experimental data for (S/S_0) intensity for C1 signal are shown in Figure 7c. The experimental data are well-consistent with the simulated curve. This result shows that helical jump motions happen in *i*P4M1P crystallites as well as in PE,[6] *i*PP,[7,8] POM,[8,9] PEO,[5] and form III of *i*PB crystallites.[10,11]

In *i*PP, it is reported that the tensor orientation of the C−CH_2−C moiety might deviate from the common direction given previously.[55] We simulate that the effect of small deviation from the common CSA tensor direction contributes to the CODEX attenuation curve. Figure 7d shows simulations assuming a σ_{22} direction deviation by +30° and −30°, respectively, from the bisection of CH_2 angle. It is obvious that the decaying behaviors are almost independent of this direction, and thus, slight disorder in the tensor direction does not seriously influence the CODEX attenuation curve. This means that CODEX data mainly depend on the jump angle and provide motional geometries without exact tensor orientations.

Spin Diffusion Correction. The NMR exchange experiment does not distinguish between molecular and spin exchange (spin diffusion).[52,56−58] In general, both

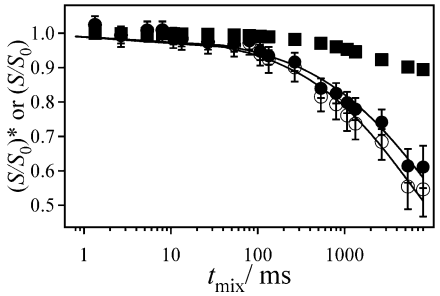

Figure 9. CODEX exchange decays for the C2 signal of *i*P4M1P crystallites before (○) and after spin diffusion correction (●) at 305 K, and the spin-diffusion curve for C2 signal (■) measured at 258 K. The solid curves are best fits to the experimental data using eq 4. The best fitted parameters of $\tau_c = 9.4 \pm 0.9$ s, $\beta = 0.55 \pm 0.03$ (●) and $\tau_c = 5.8 \pm 0.5$ s, $\beta = 0.57 \pm 0.03$ (○).

effects will be present in the exchange experiment. In typical organic compounds in natural abundance, the time constant of spin diffusion (τ_{sd}) is on the order of approximate seconds under the MAS condition.[56] Therefore, spin exchange due to spin diffusion also contributes to the exchange decay with increasing t_{mix} up to several seconds. Before discussing any kinetic parameter of helical jumps for *i*P4M1P crystallites, we need to treat the spin diffusion effect.

If the correlation time of the molecular dynamics is much shorter than that for spin diffusion ($\tau_c \ll \tau_{sd}$), we may easily separate the two effects in the exchange curve. However, in the case when correlation time for spin diffusion is in a similar order ($\tau_c \approx \tau_{sd}$) or is smaller than that for molecular dynamics ($\tau_c > \tau_{sd}$), it is difficult to separate the contributions of spin diffusion and molecular dynamics. Fortunately, the molecular process is commonly thermally activated; thus, the obtained correlation time depends on temperature. On the other hand, the spin diffusion is in a good approximation temperature independent in the regime of interest. Therefore, we can measure the pure spin diffusion effect from the exchange decay at low temperature where molecular dynamics does not contribute to the exchange decay. This signal decay due to spin diffusion is denoted as $(S/S_0)_{SD}$. Then, it is justified to extract pure the kinetic parameter as follows:[34,52]

$$(S/S_0)^* = (S/S_0)/(S/S_0)_{SD} \qquad (2)$$

In our experiments, $(S/S_0)_{SD}$ was measured at 258 K. We show an example for the spin diffusion correction in Figure 9. The mark of ■ represents (S/S_0) intensities for the C2 carbon at 258 K. The symbols ○ and ● show (S/S_0) and $(S/S_0)^*$, respectively, for the C2 carbon at 305 K. The resulting pureexchange decay curves are analyzed in terms of the following equation:

$$(S/S_0)^* = 1 - p(1 - \exp(-(t_{mix}/\tau_c)^{\beta})) \qquad (3)$$

where p is determined by the number of sites m accessible by the dynamic process, $p = (m - 1)/m$; τ_c is the correlation time; and β represents the distribution of correlation time. In the case of a diffusional process that commonly occurs in amorphous material, there is an infinite number of available sites. Therefore, p is expected to be 1, and $(S/S_0)^*$ approaches 0 at long t_{mix}. On the other hand, crystalline segments have a limited available number of sites, due to conformational restrictions and the local order in the crystalline lattice,

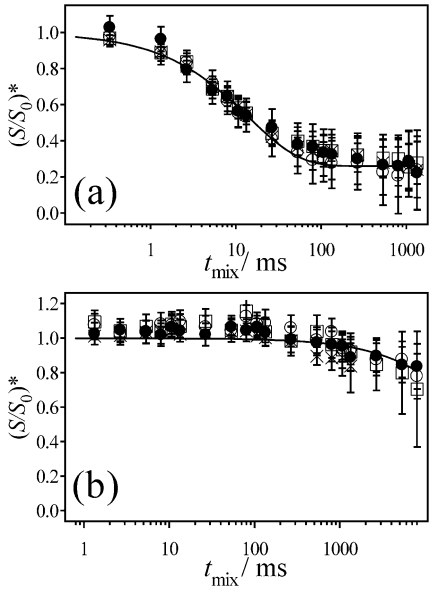

Figure 10. CODEX exchange curve of $(S/S_0)^*$ intensities for C1 (○), C2 (●), C3 (□), and C6 (×) at 360 K (a) and 299 K (b). The solid curves are best fits to the experimental data for C2 signal using eq 3.

resulting in a value of $0 < p < 1$ at t_{mix} longer than τ_c. At 305 K, (S/S_0) does not reach the equilibrium state even at a t_{mix} of 10 s. We thus used the asymptotic value, which is obtained at 360 K. The t_{mix} dependence of $(S/S_0)^*$ for C2 at 305 K is fitted with the best fitting parameters of $\tau_c = 9.4 \pm 0.9$ s and $\beta = 0.55 \pm 0.03$.

Correlation Time for Helical Jumps. Figure 10 shows t_{mix} dependencies of $(S/S_0)^*$ for all the resolved signals in *i*P4M1P crystallite at the maximum (360 K) (a) and minimum (299 K) (b) temperatures in the investigated range. At both temperatures, t_{mix} dependences of $(S/S_0)^*$ for C3 (□) and 6 (×) in the side chain almost match those for the main-chain signals C1 (○) and C2 (●) within the experimental errors. The plateau values for the main chain are in agreement with those of the side chain, too. These evidences indicate that the side chain moves in concert with the main chain in the crystallites, and there are no slow independent motions. Kinetic parameters are obtained for the helical jump of the C2 signal from the fitting of the t_{mix} dependence using eq 3. At 360 K, the fitting of $(S/S_0)^*$ of C2 yields $p = 0.70 \pm 0.12$, $\tau_c = 13.9 \pm 1.3$ ms, and $\beta = 0.71 \pm 0.11$. As mentioned in the previous section, the p value is directly related to the available site number, m. In *i*P4M1P crystallites, if all the segments participate in the helical jump, a value of $p = 0.86$ is expected. The experimental asymptotic value, 0.70, is actually slightly smaller than the expected value. This means that about 81% crystalline segments participate in the helical jump motions.

Below 327 K, $(S/S_0)^*$ does not reach a plateau within the available t_{mix}, and the kinetic parameters were obtained assuming $p = 0.70$. We obtain $\tau_c = 31.2 \pm 22.1$ s and $\beta = 0.71 \pm 0.22$ for C2 at 299 K as shown in Figure 10b. The correlation times for helical jump motions obtained through the C2 signal (●) are plotted in Figure 11. The dotted lines are best Arrhenius fits to the experimental data above 316 K, with $E_a = 95.2 \pm 5.3$ kJ/mol, and show the deviation of the correlation times from the Arrhenius behavior with decreasing temperature. Such a behavior is known from segmental motions in amorphous polymers, which are associated with

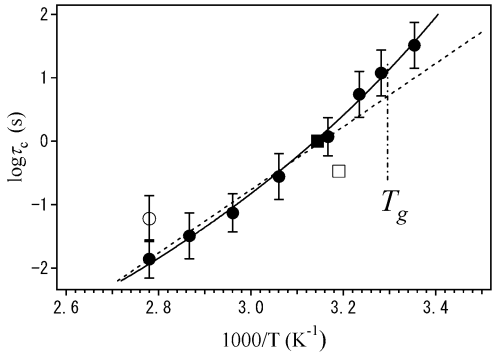

Figure 11. Arrhenius diagram of the correlation times for helical jump motions (●) and conformational transition (○) of *i*P4M1P crystallites obtained by CODEX and 2-D exchange NMR, respectively. The bars mean a distribution width for the correlation times, assuming a log Gaussian distribution. The mechanical data of *i*P4M1P by Reddy et al.[21] and Datch[22] are also shown as ■ and □, respectively. The broken line shows a best fitted one with activation energy of 95.2 ± 5.3 kJ/mol (note the deviation at low temperatures). The solid curve shows WLF one with best fitted parameters of $C_1 = 8.4 \pm 1.2$, $C_2 = 75 \pm 17$ K, and $T_s = 294 \pm 3$ K. The short-dashed and dotted line shows the T_g in our sample, which was determined by DSC.

T_g. The non-Arrhenius dependence of the correlation time is expressed in the following WLF equation:[59]

$$\tau(T) = \tau_s \exp(-2.303C_1(T - T_s)/(C_2 + (T - T_s))) \quad (4)$$

where C_1 and C_2 are empirical parameters.[60] τ_s is the correlation time at reference temperature T_s. In the α process of amorphous polymers, T_g is identified with the temperature at which the correlation time equals a characteristic value of 10^2 s. We thus apply a correlation time of 10^2 s at a reference temperature, T_s, to the experimental data of *i*P4M1P crystallites. The fitted curve shows the best fit one with parameters of $C_1 = 8.4 \pm 1.2$, $C_2 = 75 \pm 17$ K, and $T_s = 294 \pm 3$ K. The WLF function is equivalent to the Vogel−Fulcher−Tammann(−Hesse) (VFT) equation[61]

$$\tau(T) = \tau_0 \exp(-DT_0/(T - T_0)) \quad (5)$$

with $T_0 = T_s - C_2$, $DT_0 = 2.303C_1C_2$, and $\tau_0 = \tau_s \exp(-2.303C_1)$. The parameter D tells how closely the system obeys the Arrhenius behavior.[62,63] The fragile glassy polymers show large deviations from the Arrhenius law, corresponding to small values of $D < 10$. On the other hand, it is graphically difficult to distinguish WLF (VFT) behavior from the Arrhenius one under $D \geq 100$. The obtained WLF parameters show $D = 7 \pm 2$ for *i*P4M1P crystallites.

Discussion

Glass Transition Temperature. Most of the previous investigations indicated that the observed mechanical peaks around 293−323 K originate from segmental motions in the amorphous regions.[17−20,22] In the latest investigation, Reddy et al. observed ^{1}H line widths through the resolved ^{13}C signals at 293 and 373 K by ^{1}H-^{13}C WISE NMR experiments, and only the C6 signal in the amorphous region shows an ^{1}H narrowed signal at 373 K. Then, they corrected the observed mechanical peak at 318 K by DMA due to the side-chain motion in the amorphous regions.[21] Our ^{13}C CPMAS spectra show the C6 signal in the amorphous region above 404 K, as Reddy observed previously. Moreover, our CPMAS and relaxation experiments at various temperatures show that the segmental motions in the amorphous region show correlation times in the order of 0.2×10^{-5} s at 360−382 K, and the DSC result shows that there is an apparent heat-capacity jump between 290 and 318 K, which is the typical indication of T_g for polymers. We, therefore, have to reject Reddy's conclusion and conclude that the center temperature (304 K) in the DSC baseline change is T_g of our sample and that the previously observed mechanical peaks at 293−323 K are also due to the α_a relaxation.[17−20,22]

Griffith et al. investigated T_g of *i*P4M1P as a function of crystallinity by specific volume versus temperature measurements.[17] They indicated that the T_g value decreases with increasing crystallinity. This behavior is anomalous in the semicrystalline polymers; however, it can be reasonably well-understood by our experimental result on the dynamic behavior in the crystalline region.

Helical Jump Motion around T_g. The crystalline polymers such as PE,[6] POM,[8,9] and *i*PP[7,8] show similar large amplitude motions at a much higher temperature than their T_g, and their dynamics shows Arrhenius-type behavior of the temperature dependence of correlation times. On the other hand, the temperature dependence of correlation times for the helical jump motions of *i*P4M1P shows non-Arrhenius behavior, and the onset temperature (T_g − 10 K) is slightly lower than T_g (Figure 11). This kind of dynamic behavior is anomalous in semicrystalline polymers. There are two possible reasons for the observed WLF behavior: (1) a disordered crystal and (2) constraint from amorphous immobility below T_g. There are a number of dynamic investigations in polymer crystallites by solid-state NMR; however, only one detailed dynamics investigation on time parameters for *atactic*-poly(acrylonitrile) (*a*-PAN) in disordered crystals was very recently performed by Kaji et al.[64] They evidently show that *a*-PAN exhibit uniaxially rotational motions with large amplitudes, and their correlation times obey Arrhenius behavior. This result suggests that even disordered polymer crystals show an Arrhenius type of dynamics.

In the case of the semicrystalline polymers, the polymer chains extend in both the amorphous and in the crystalline regions. The helical jump motion includes a chain translation along the *c* axis. Therefore, some segments diffuse between the crystalline and the interfacial and/or amorphous regions. In PE, such chain diffusion was experimentally observed at a much higher temperature than T_g[12] and near the α_c relaxation temperature. At such temperatures, the polymer chains in the amorphous and/or interfacial regions show higher mobility than those in the crystalline regions. Consequently, it is likely that high mobility in the amorphous region leads to easy chain diffusion between the crystalline and the amorphous regions. This situation holds for *i*PP and POM and leads to the Arrhenius-type of motions in the crystalline region. On the other hand, for *i*P4M1P crystallites, the reference temperature, $T_s = 294$ K, of the helical jump motion is slightly lower than T_g at which the segmental mobility in the amorphous region steeply slows down. Under this condition, immobility of the amorphous parts restricts the translational motions of the crystalline segments and consequently leads to the observed amorphous-like WLF behavior. The obtained and small D value of 7 is

consistent with those for typical amorphous polymers, $D < 10$,[62,63] and indicates a strong effect from the amorphous constraint.

Conformationally Disordered Crystals versus Conformationally Uniform Crystals. 2-D MAS exchange NMR revealed that conformational transition for the main chains in the crystalline region occurs in the same order of correlation time (○) with that for helical jumps (●) at 360 K (see Figure 11). From this evidence, it can be safely concluded that helical jump motions and conformational transitions are not independent, and the former process induces the latter in the conformationally disordered seven sites. Such a direct observation for conformational transition evidently shows that *i*P4M1P is one of the conformationally disordered (CONDIS) crystals.[65,66] Under the presence of helical jump motions, the continuous and minor downfield shifts of all the signals are also observed above 299 K (Figure 3). The σ_{iso} change can be interpreted as a minor change in the averaged conformation and packing structure. Here, we consider a relation between structure and dynamics. The chain conformation and packing in the crystalline lattice are influenced by a packing relation with the neighboring chain. If each polymer chain performs helical jumps completely cooperative with the neighboring chains, conformational transition happens uniformly over an individual helix, and it would result in averaged σ_{iso} values. If there is dynamic disorder with the nearest chains, such dynamic disorder might cause conformational and/or packing structure change, and consequently, leads to σ_{iso} shifts.

There are several dynamics investigations on CONDIS and uniform polymer crystals. Here, we compare dynamic character in both. In the former, the PEO crystal has a 7_2 helical structure, and the conformations in each site slightly deviates from the ideal one.[67] ^{13}C CPMAS NMR spectrum shows asymmetric line shape depending on the disordered 7_2 helical structures at low temperature where helical jump motions do not influence the line shape.[68] ^{13}C 2-D exchange NMR pattern was not completely consistent with the simulation reproduced by the jump motions on the basis of the crystalline structures. It was suggested that the PEO crystallite shows long-range disorder in the static structure, which was determined by WAXD.[5]

a-PAN is also a CONDIS crystal due to a configuration disorder. WAXD investigation shows the crystal shows only lateral order, meaning that there is disorder along the *c* axis.[69] Kaji et al. investigated structures and dynamics of *a*-PAN using advanced NMR techniques.[64,70−72] It was revealed that *a*-PAN does show not discrete jump motions but shows uniaxially rotational motions with a large distribution of the jump angles in space, and this deviation angle increases as a function of temperature.

In contrast, PE and *i*PP have uniform conformations, although 1-D and 2-D exchange NMR reveal a distribution of correlation times of the large amplitude motions.[6,31] 2-D exchange NMR results and their simulations show PE and *i*PP perform jumps with ideal jump angles on the basis of crystalline structures.[6−8] Furthermore, ^{13}C isotropic chemical shifts of PE and *i*PP crystallites are almost invariant in the α_c relaxation temperature range.[13,14,73]

These previous findings and our results indicate that the heterogeneity in kinetic parameters of the overall motions is common in CODIS and uniform crystals; however, conformational changes or heterogeneity in amplitude of motions occur only in the conformationally disordered polymer crystal. These structural and dynamic changes would originate from dynamic disorders with the neighboring chains and/or configuration disorder.

In addition, it would be interesting to compare the side- and main-chain dynamics of *i*P4M1P crystallites with those for amorphous polymers having side chains. As discussed previously, *i*P4M1P crystalline segments show no independent side-chain motions and only helical jump motions in the restricted spaces. Several authors investigated the main- and side-chain dynamics for PaMA with different side-chain lengths around T_g.[52,74−76] In PaMA, the side groups commonly show 180° flipping motions, and the fraction of the flipping groups increases with temperature.[74,75] The main chains show a partially extended structure due to the polar COO groups even for the amorphous polymer, and the main chains show restricted axial chain motions, which are strongly coupled to the side-chain motions.[52,74,75] The motional amplitude of the chain motions increases with temperature, and the main-chains retain conformations and orientations over many steps of axial motions. Very recently, Wind et al. found that randomization of conformations and isotropization of the chains in PaMA occur at the temperature where axial rotations occur but shows a much slower process than the slowest dynamic process identified so far.[76] These dynamics are in contrast to the chain dynamics of *i*P4M1P in the crystalline lattice.

Several authors investigated thermal expansion coefficients of the unit cell parameters for *i*P4M1P[19,23] and assigned the change in thermal expansion coefficient to the onset of the chain dynamics in the crystalline regions. If helical jump motion does occur in the available sites in the rigid case, the motion does not contribute to the thermal expansion coefficient. In the case of *i*P4M1P, the dynamic disorder of the helical jump induces conformational and/or packing structure change, and consequently, leads to variations of unit cell parameters with temperature. The observed change in the unit cell parameter around 303 K[19] was originally attributed to T_g. From our NMR analysis, it should be revised as changes of unit cell parameters should be attributed to the dynamic disorder of the helical jump motions in the *i*P4M1P crystalline regions.

Comparison between Our NMR and Mechanical Data. Here, we compare our NMR results with previously reported mechanical data.[17−22] So far, a number of authors investigated the mechanical property of *i*P4M1P by DMA. We plotted in Figure 11 the lower temperature relaxations, which were recently observed by Reddy et al.[21] and Datch,[22] respectively. The obtained correlation times from our investigation of helical jump motions are very close to the mechanical relaxations. As mentioned previously, T_g for the sample in the present work is 304 K. Therefore, segmental motions in the amorphous region and helical jump motions in the crystalline region contribute to the lower temperature relaxations around 293−323 K, which should be corrected to be a combination of α_a and α_c (α_{a+c}). This conclusion is exceptional for chain dynamics in the semicrystalline polymers; however, it should be reasonably accepted in the light of the unusual density property for *i*P4M1P.

Datch and several other authors also investigated the higher temperature relaxations at 403−433 K. These were assigned to α_c relaxation on the basis of the general concept that the α_c relaxation occurs at much higher temperature than α_a relaxation. These peaks, however, are very broad and weak. From our CODEX data, we estimated the correction time for the helical jump motions to be 0.3×10^{-5} s at 420 K. 1-D ^{13}C CPMAS spectra and $T_{1\rho c}$ results permit the estimate that the segmental motions in the crystalline and amorphous regions reach the correlation times of and those over 0.2×10^{-5} s at 448 and 360−382 K, respectively. These NMR evidences deny α_c relaxation with a frequency of several Hz around 403−433 K. Furthermore, this conclusion is supported by the mechanical data obtained by Reddy et al.[21] and Griffith et al.[17] The former observed only one mechanical peak up to 453 K, and the latter showed that the mechanical peak at the higher temperature process disappears with increasing crystallinity.

Conclusions

We characterized in detail the chain dynamics in the crystalline region of *i*P4M1P in natural abundance by CODEX NMR experiments with $T_{1\rho c}$ relaxation filter in the correlation time range of 10^{-2} to 10^2 s, which covers the typical α_c relaxation range. It was demonstrated that *i*P4M1P crystallites start helical jump motions at temperatures slightly lower than T_g, and the temperature dependence of the correlation times obey WLF behavior with a reference temperature, $T_s = 294$ K. The strong slowing down of the correlation times near T_g indicates a correlation between the chain dynamics of crystalline and amorphous region, and the crystalline dynamics is restricted by the amorphous immobility. From this evidence, we correct the previously reported α_a relaxation at 293−323 K to α_{a+c} relaxation. Furthermore, we need to question the general concept that α_c relaxation occurs at much higher temperature than α_a relaxation. This finding is an exceptional aspect for crystalline dynamics. However, this unusual dynamic behavior could be reasonably explained by the unusual density property of *i*P4M1P and might be characteristic for the semicrystalline polymers with long side chains.

Acknowledgment. T.M. thanks NEDO (New Energy and Industrial Technology Development Organization) in the framework of Nanostructure Polymer Project. O.P. and D.R. thank the Deutsche Forschungsgemeinschaft DFG in the frame of SFB 418 for financial support.

References and Notes

(1) Boyd, R. H. *Polymer* **1985**, *26*, 383−347.
(2) Men, Y.; Rieger, J.; Endeler, H. F.; Lilge, D. *Macromolecules* **2003**, *36*, 4689−4691.
(3) Mano, J. F. *Macromolecules* **2001**, *34*, 8825−8828.
(4) Hu, W. G.; Schmidt-Rohr, K. *Acta Polym.* **1999**, *50*, 271−285.
(5) Schmidt-Rohr, K.; Spiess, H. W. *Multidimensional Solid-State NMR and Polymers*; Academic Press: London, 1994.
(6) Hu, W. G.; Boeffel, C.; Schmidt-Rohr, K. *Macromolecules* **1999**, *32*, 1611−1619.
(7) Schaefer, D.; Spiess, H. W.; Suter, U. W.; Fleming, W. W. *Macromolecules* **1990**, *23*, 3431−3439.
(8) Hagemeyer, A.; Schmidt-Rohr, K.; Spiess, H. W. *Adv. Magn. Reson.* **1989**, *13*, 85−130.
(9) Kentgens, A. P. M.; de Boer, E.; Veeman, W. S. *J. Chem. Phys.* **1987**, *87*, 6859−6866.
(10) Maring, D.; Whilhelm, M.; Spiess, H. W.; Meurer, B.; Weill, G. *J. Polym. Sci., Part B: Polym. Phys.* **2000**, *38*, 2611−2624.
(11) Miyoshi, T.; Hayashi, S.; Imashiro, F.; Kaito, A. *Macromolecules* **2002**, *35*, 2624−2632.
(12) Schmidth-Rohr, K.; Spiess, H. W. *Macromolecules* **1991**, *24*, 5298−5306.
(13) Kuwabara, K.; Kaji, H.; Horii, F. *Macromolecules* **2000**, *33*, 4453−4462.
(14) Kuwabara, K.; Kaji, H.; Horii, F. *Macromolecules* **2000**, *33*, 7093−7110.
(15) Kusanagi, H.; Takase, M.; Chatani, Y.; Tadokoro, H. *J. Polym. Sci., Part B: Polym. Phys.* **1978**, *16*, 131−142.
(16) Zanuy, D.; Alemán, C.; Munoz-Guerra, S. *J. Polym. Sci., Part B: Polym. Phys.* **2002**, *40*, 2037−2049.
(17) Griffith, J. H.; Randy, B. G. *J. Polym. Sci.* **1960**, *44*, 369−381.
(18) Takayanagi, M.; Kawasaki, N. *J. Macromol. Sci., Polym. Phys. Ed.* **1967**, *B1*, 741−758.
(19) Tanigami, T.; Yamaura, K.; Matsuzawa, S.; Miyasaka, K. *Polym. J.* **1986**, *18*, 35−40.
(20) Choy, L. C.; Luk, W. K.; Chen, F. C. *Polymer* **1981**, *22*, 543−548.
(21) Reddy, S.; Desai, P.; Abhiraman, A. S.; Beckham, H. W.; Kulik, A. S.; Spiess, H. W. *Macromolecules* **1997**, *30*, 3293−3301.
(22) Datch, A. *J. Therm. Anal.* **1998**, *54*, 151−159.
(23) Nakamae, K.; Nishino, T.; Takagi, S. *J. Macromol. Sci., Phys.* **1991**, *B30*, 47−62.
(24) Woodward, A. E.; Odajima, A.; Sauer, A. J. *J. Phys. Chem.* **1961**, *65*, 1384−1391.
(25) Chan, S. K.; Randy, G.; Brumberger, H.; Odajima, A. *J. Polym. Sci.* **1962**, *61*, S29.
(26) Yang, Y.; Schuster, M.; Blumich, B.; Spiess, H. W. *Chem. Phys. Lett.* **1987**, *139*, 239−243.
(27) Gerardy-Montouilout, V.; Malveau, C.; Tekely, P.; Olender, Z.; Luz, Z. *J. Magn. Reson.* **1996**, *123*, 7−15.
(28) Reichert, D.; Zimmermann, H.; Tekely, P.; Olender, Z.; Luz, Z. *J. Magn. Reson.* **1997**, *125*, 245−258.
(29) Reichert, D.; Hempel, G.; Luz, Z.; Tekely, P.; Schneider, H. *J. Magn. Reson.* **2000**, *146*, 310−320.
(30) Reichert, D.; Pascui, O.; Beiner, M. *Macromol. Symp.* **2002**, *184*, 175−181.
(31) deAzevedo, E. R.; Hu, W. G.; Bonagamba, T. J.; Schmidt-Rohr, K. *J. Am. Chem. Soc.* **1999**, *121*, 8411−8412.
(32) deAzevedo, E. R.; Hu, W. G.; Bonagamba, T. J.; Schmidt-Rohr, K. *J. Chem. Phys.* **2000**, *112*, 8988−9001.
(33) Reichert, D.; Pascui, O.; Bonagamba, T. J.; deAzevedo, E. R.; Schmidt, A. *Chem. Phys. Lett.* **2003**, *380*, 583−588.
(34) Miyoshi, T.; Pascui, O.; Reichert, D. *Macromolecules* **2002**, *35*, 7178−7181.
(35) Charlet, G.; Delmas, G. *Polymer* **1984**, *25*, 1619−1625.
(36) Charlet, G.; Delmas, G.; Revol, F. J.; Manley, J. S. *Polymer* **1984**, *25*, 1613−1618.
(37) Lopez, L. C.; Wilkes, G. L.; Stricklen, P. M.; White, S. A. *J. Macromol. Sci., Chem.* **1992**, *32*, 301−406.
(38) Zoller, P.; Howard, W.; Strakweather, W.; Jones, G. A. *J. Polym. Sci., Part B: Polym. Phys.* **1986**, *24*, 1451−1458.
(39) Bielecki, A.; Burum, D. P. *J. Magn. Reson. A* **1995**, *116*, 215−220.
(40) Takahashi, T.; Kawashima, H.; Sugisawa, H.; Baba, T. *Solid-State NMR* **1999**, *15*, 119−123.
(41) Bennet, A. E.; Rienstra, C. M.; Auger, M.; Lakshmi, K. V.; Griffin, R. G. *J. Chem. Phys.* **1995**, *103*, 6951−6958.
(42) Liu, S. F.; Mao, J. D.; Schmidt-Rohr, K. *J. Magn. Reson.* **2002**, *155*, 15−28.
(43) De Rosa, C.; Capotani, D.; Cosco, S. *Macromolecules* **1997**, *30*, 8322−8331.
(44) Tonelli, A. E. *NMR Spectrocscopy and Polymer Microstructure: The Conformaitonal Connection*; VCH Publishers: New York, 1989.
(45) Zemke, K.; Schmidt-Rohr, K.; Spiess, H. W. *Acta Polym.* **1994**, *45*, 148−159.
(46) VanderHart, D. L.; Earl, W. P.; Garroway, A. N. *J. Magn. Reson.* **1981**, *44*, 361−401
(47) Rothwell, W. P.; Waugh, J. S. *J. Chem. Phys.* **1981**, *74*, 2721−2732.
(48) Schaefer, J.; Stejskal, E. O.; Buchdahl, R. *Macromolecules* **1978**, *10*, 384−405.
(49) Schaefer, J.; Stejscal, E. O.; Steger, T. R.; Sefcic, M. D.; Mckay, R. A. *Macromolecules* **1980**, *13*, 1121−1126.
(50) VanderHart, D. L.; Garroway, A. N. *J. Chem. Phys.* **1979**, *71*, 2773−2787.
(51) Yamaguchi, M.; Tsutsumi, A. *Polym. J.* **1993**, *25*, 427−433.
(52) Pascui, O.; Beiner, M.; Reichert, D. *Macromolecules* **2003**, *36*, 3992−4003.

(53) Schmidt-Rohr, K.; Whilhelm, M.; Johansson, A.; Spiess, H. W. *Magn. Reson. Chem.* **1993**, *31*, 352−356.
(54) Dunbar, M. G.; Novak, B. M.; Schmidt-Rohr, K. *Solid-State NMR* **1998**, *12*, 119−137.
(55) Nakai, T.; Asida, J.; Terao, T. *Magn. Reson. Chem.* **1989**, *27*, 666−668.
(56) Reichert, D.; Hempel, G.; Zimmermann, H.; Tekely, P.; Poupko, R.; Luz, Z.; Favre, D. E.; Chmelka, B. F. *Appl. Magn. Reson.* **1999**, *17*, 315−327.
(57) Tekely, P.; Gardiennet, C.; Potrzebowski, M.; Sebald, A.; Reichert, D.; Luz, Z. *J. Chem. Phys.* **2002**, *116*, 7607−7616.
(58) Reichert, D.; Bonagamba, T.; Schmidt-Rohr, K. *J. Magn. Reson.* **2001**, *151*, 129−135.
(59) Williams, M. L.; Landel, R. F.; Ferry, J. D. *J. Am. Chem. Soc.* **1955**, *77*, 3701−3707.
(60) Strobl, G. R. *The Physics of Polymers*; Springer: Berlin, 1996.
(61) McGrum, N. G.; Read, B. E.; Williams, G. *Anelastic and Dielectric Effects in Polymer Solids*; Wiley: New York, 1967.
(62) Angell, C. A. *Science* **1995**, *267*, 1924−1935.
(63) Böhmer, R.; Ngai, K. L.; Anell, C. A.; Plazek, D. J. *J. Chem. Phys.* **1993**, *99*, 4201−4209.
(64) Kaji, H.; Miura, N.; Schmidt-Rohr, K. *Macromolecules* **2003**, *36*, 6100−6113.
(65) Wunderlich, B.; Moller, M.; Grebowicz, J.; Baur, H. *Advances in Polymer Science*; Springer-Verlag: Berlin, 1988; Vol. 87.
(66) Unger, G. *Polymer* **1993**, *34*, 2050−2059.
(67) Takahashi, Y.; Tadokoro, H. *Macromolecules* **1973**, *6*, 672−675.
(68) Schilling, F. C.; Tonelli, A. E.; Cholli, A. L. *J. Polym. Sci., Part B: Polym. Phys.* **1992**, *30*, 91−96.
(69) Rizzo, P.; Auriemma, F.; Guerra, G.; Petraccone, V.; Corradini, P. *Macromolecules* **1996**, *29*, 8852−8861.
(70) Kaji, H.; Schmidt-Rohr, K. *Macromolecules* **2000**, *33*, 5169−5180.
(71) Kaji, H.; Schmidt-Rohr, K. *Macromolecules* **2001**, *34*, 7368−7381.
(72) Kaji, H.; Schmidt-Rohr, K. *Macromolecules* **2001**, *34*, 7382−7391.
(73) Saito, S.; Moteki, Y.; Nakagawa, M.; Horii, F.; Kitamaru, R. *Macromolecules* **1990**, *23*, 3256−3260.
(74) Kulik, A. S.; Beckham, W. W.; Schmidt-Rohr, H. W.; Ohlemacher, A.; Pawelzik, U.; Boeffel, C.; Spiess, H. W. *Macromolecules* **1994**, *27*, 4746−4754.
(75) Bonagamba, T. J.; Becker-Guedes, F.; deAzevedo, E. R.; Schmidt-Rohr, K. *J. Polym. Sci., Part B: Polym. Phys.* **2001**, *39*, 2444−2453.
(76) Wind, M.; Graf, R.; Heuer, A.; Spiess, H. W. *Phys. Rev. Lett.* **2003**, *91*, 155702−155705.

MA049487C